

# Unraveling the Structure of Ultracold Mesoscopic Molecular Ions

J. M. Schurer,\* A. Negretti, and P. Schmelcher†

Zentrum für Optische Quantentechnologien, Universität Hamburg,  
Luruper Chaussee 149, 22761 Hamburg, Germany and  
The Hamburg Centre for Ultrafast Imaging, Universität Hamburg,  
Luruper Chaussee 149, 22761 Hamburg, Germany

(Dated: April 9, 2021)

We present an in-depth many-body investigation of the so-called mesoscopic molecular ions that can build-up when an ion is immersed into an atomic Bose-Einstein condensate in one dimension. To this end, we employ the Multi-Layer Multi-Configuration Time-Dependent Hartree method for Mixtures of ultracold bosonic species for solving the underlying many-body Schrödinger equation. This enables us to unravel the actual structure of such massive charged molecules from a microscopic perspective. Laying out their phase diagram with respect to atom number and interatomic interaction strength, we determine the maximal number of atoms bound to the ion and reveal spatial densities and molecular properties. Interestingly, we observe a strong interaction-induced localization, especially for the ion, that we explain by the generation of a large effective mass, similarly to ions in liquid Helium. Finally, we predict the dynamical response of the ion to small perturbations. Our results provide clear evidence for the importance of quantum correlations, as we demonstrate by benchmarking them with wave function ansatz classes employed in the literature.

*Introduction.*— In early studies on ions in liquid  $^4\text{He}$ , a small ionic mobility in the liquid was detected experimentally [1]. To explain this observation, a high liquid density around the ion was suggested [2]. The latter was subsequently corroborated by the generation of a large effective mass for the ionic impurity [3], as many atoms are attracted to the ion. In recent years, the combination of degenerate quantum gases and trapped ions has opened new perspectives [4] thereby allowing to explore the underlying mechanisms of such phenomena. Indeed, the exquisite controllability of both quantum gases and trapped ions enable in-depth investigations of fundamental processes ranging from ultracold chemical reactions [5–7], charge transport [8], and spin decoherence [9] to sympathetic cooling [7, 10, 11] and the strong-coupling regime of polaron physics [12]. Importantly, the atom-ion interaction supports the formation of weakly-bound charged dimers with binding radii of hundreds of nanometers or more [13] which can be formed by three-body collisions [14, 15] or radiative processes [6]. These molecules are reminiscent of Feshbach or halo molecules [16–18] as their neutral counterparts are named and represent an example for extraordinary molecules with a binding radius and a de-Broglie wave length of the same order of magnitude. Even more fascinating, they can consist of multiple bosonic atoms and a single ion, such that they become mesoscopic massive quantum objects [13], eventually even exhibiting a shell structure [19]. When no population of the bound states occurs, a single tightly confined ion is predicted to induce a micron sized density disturbance with hundreds of excess atoms in an ultracold gas [3, 20] which becomes a clear density hole in the Tonks-Girardeau limit [21]. However, such a density hole increasingly closes if bound states become populated [22].

In this work, we explore the quantum state of such mesoscopic molecular ions in one spatial dimension (1D)

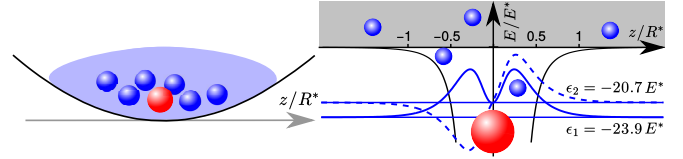


FIG. 1. (Color online) Setup and atom-ion interaction. (Left) Atoms (blue) and ion (red) in a quasi one-dimensional harmonic trap. (Right) Atom-ion interaction potential (solid black line) together with the two most weakly bound states and their energies  $\epsilon_i$ ; bound and unbound atoms are indicated.

based on a microscopic theory (see Fig. 1). Thereby, we are able to derive a complete zero-temperature phase diagram for the compound system and show how strongly the critical cluster size [13] is affected when particle correlations are taken into account. We confirm the hypothesis of interatomic interaction-induced excitations stabilizing the molecular cluster [19] and observe as well as explain the self-localization behavior of the ion, which becomes possible by incorporating the ionic motional degree of freedom, not taken into account in earlier studies [20–25]. As a result, we connect the atomic density profiles, in particular the predicted density hole [20–22], with the spatial extent of the ionic wave function and predict the dynamical response of the ion to a small perturbation. All this is attained by exploiting the knowledge of the numerically computed many-body correlated quantum state of the compound system and allows to benchmark commonly used wave function ansatz classes.

*Setup.*— We study a single ion of mass  $m$  and position  $z_i$  immersed into a cloud of  $N$  bosonic ultracold atoms of mass  $m$  located at  $z_i$  both confined in a harmonic trap of frequency  $\omega$ . Let us remark that the choice of equal trap frequencies is for reasons of simplicity and our results

(see below) do generalize to the case of unequal trapping frequencies. The atoms interact via a contact-interaction potential of strength  $g$ , while the atom-ion interaction is given by  $V_{\text{AI}}(z_i - z_1) = -\frac{1}{2}\alpha e^2(z_i - z_1)^{-4}$  [26] with the atomic polarizability  $\alpha$  inducing a characteristic length  $R^* = \sqrt{\alpha e^2 m / (2\hbar^2)}$  and energy  $E^* = \hbar^2 / (mR^{*2})$  scale. Moreover, we take the two most weakly bound states of the atom-ion interaction into account (see Fig. 1) which are eigenstates of the relative Hamiltonian  $-(\hbar^2/m)\partial_r^2 + V_{\text{AI}}(r)$  with energy  $\epsilon_i$ . In order to reveal the physics originating from the atom-ion interaction, we set the trap length  $l = \sqrt{\hbar/(m\omega)} = R^*$ .

*Phase Diagram.*— Depending on  $N$  and  $g$ , two distinct phases for the ground state occur (see Fig. 2), which can be separated by looking at the sign of the chemical potential

$$\mu = E(N+1, g) - E(N, g) \quad (1)$$

with the total energy  $E(N, g)$ . For  $\mu < 0$ , the presence of the bound states makes the binding of all bosonic atoms possible such that a single *mesoscopic charged molecule* is formed. The near linear decrease of  $E(N)$  (inset) shows that the atoms are “inserted one by one” into the bound state, which is only possible due to their bosonic nature. In contrast, for  $\mu > 0$ , the total energy can not be reduced anymore by adding another atom. This clearly indicates that not all atoms can be bound, since the ion becomes increasingly screened, resulting in an unbound, yet trapped, atomic fraction. In between these two regimes, the *dissociation* of the molecule occurs at  $\mu = 0$  defining the maximal number of atoms  $N_c$  that can be bound to the ion for a fixed  $g$ . Hence, we find a transition from an all-bound many-body state to a molecule immersed into an unbound background gas. One can estimate the threshold region by energetic considerations to be  $g_c \approx (\omega - \epsilon_1)/(N_c - 1)$  (see Fig. 2 dashed line).

The question which arises now is: How to capture the essential nature of such a many-body quantum state, particularly from microscopic considerations? A natural starting point for the theoretical description of the wave function  $|\Psi\rangle$  is obtained by variationally optimizing a product ansatz

$$\Psi_{\text{MF}}(z_1, z_1, \dots, z_N) = \varphi(z_1) \prod_{i=1}^N \chi(z_i), \quad \text{or} \quad (2)$$

$$\Psi_{\text{G}}(Z_1, Z_1, \dots, Z_N) = \varphi(Z_1) \prod_{i=1}^N \chi(Z_i). \quad (3)$$

The first ansatz  $\Psi_{\text{MF}}$  corresponds to a product of the atomic and the ionic part of the wave function together with a Gross-Pitaevskii ansatz for the atomic part. Hence, we refer to this ansatz as mean-field (MF). The second ansatz  $\Psi_{\text{G}}$ , inspired by Gross [3], is a product in the ion-frame (IF) coordinates  $Z_1 = z_1$  and  $Z_i = z_i - z_1$ . In order to go even beyond

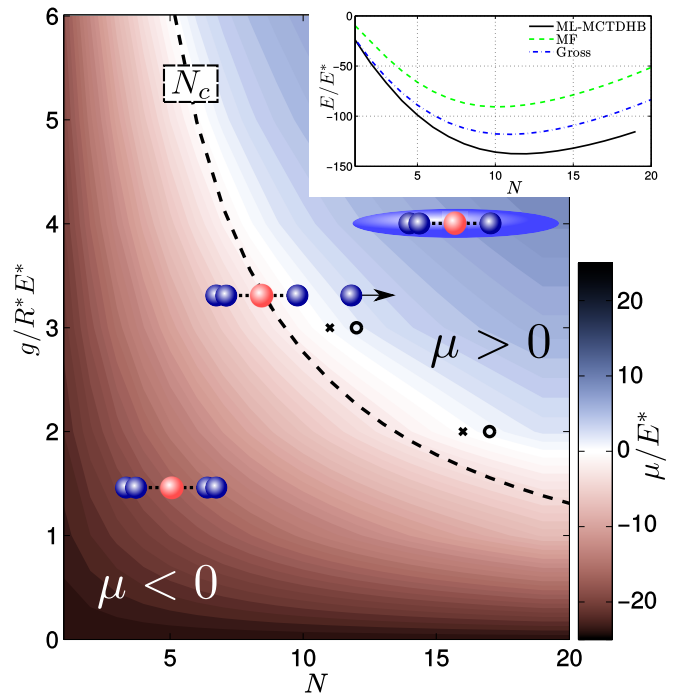


FIG. 2. (Color online) Phase diagram. Chemical potential  $\mu$  from the Gross ansatz as a function of  $N$  and  $g$ . Black circle (crosses) mark  $\mu = 0$  from ML-MCTDHB (Gross). The black dashed line presents the estimation  $g_c \approx (\omega - \epsilon_1)/(N_c - 1)$ . (Inset) Total energy  $E(N)$  as a function of  $N$  for  $g = 3E^*R^*$ .

both ansatz wave functions, we employ the multi-layer multi-configuration time-dependent Hartree method for bosons (ML-MCTDHB) [27, 28] (see Supplemental Material [26]), which allows us to numerically compute the ground state of the hybrid system via imaginary time-propagation, i.e. relaxation. We observe that the MF can reproduce a minimum in the total energy (see inset of Fig. 2), nevertheless it predicts a substantially too large energy. The Gross ansatz already lowers the total energy hence is closer to the true ground state due to the underlying variational principle. The ML-MCTDHB results, however, further approach the true many-body ground state such that we can use them to benchmark the MF and the Gross approach. In addition to the lowering of  $E(N)$ , it also predicts the dissociation at larger  $N$  (c.f. circle and crosses).

*Molecular Structure.*— In order to unravel the structure of such a many-body state, we begin with the atomic and ionic density profiles  $\rho_{\text{I(A)}}(z) = \langle \hat{\Psi}_{\text{I(A)}}^\dagger(z) \hat{\Psi}_{\text{I(A)}}(z) \rangle$  (see Fig. 3) where  $\hat{\Psi}_{\text{I(A)}}$  are the ion (atom) field operators. We observe that for small  $N$  both density distributions are of similar shape and spatial extension though with different maximal values. For large  $N$ , the ion becomes significantly localized, while the atoms reveal two peaks in the density ( $g = 0$ ) and exhibit the formation of broad shoulders ( $g > 0$ ). We observe that the qualitative behavior of the latter can be captured by a Thomas-

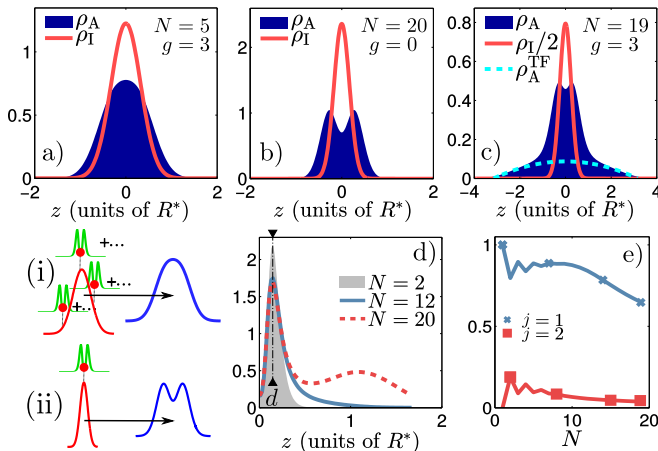


FIG. 3. (Color online) Molecular structure. (a-c) Atomic (shaded) and ionic (solid line) density profiles. In (c) also a Thomas-Fermi profile with  $N - N_c$  particles is shown (dashed line). (d) Atom-ion correlation function  $g_2(z)$  for  $g = 3R^*E^*$ . (e) Population of the bound states  $f_j/N$ . (i) Delocalized versus (ii) localized ion and its impact on the atomic density.

Fermi (TF) profile with  $N_{\text{TF}} = N - N_c$  atoms (cyan line). However, we emphasize that the atoms are strongly correlated and far away from the validity regime of the TF approximation. The fact that the atoms are bound or unbound is, however, not obvious from the density profiles and becomes only explicit in the atom-ion correlation function

$$g_2(z) = \frac{\langle \hat{\Psi}_I^\dagger(z) \hat{\Psi}_A^\dagger(-z) \hat{\Psi}_A(-z) \hat{\Psi}_I(z) \rangle}{N \rho_I(z) \rho_A(-z)} \quad (4)$$

with  $z = z_A - z_I$  shown in Fig. 3 d). Here, we can clearly see that it is most likely to find an atom at the binding distance  $d$  (vertical dashed line) from the ion, while larger distances are strongly suppressed for  $N < N_c$  ( $N_c = 12$  for  $g = 3E^*R^*$ ). Note that the MF ansatz results in  $g_2(z_A - z_I) = 1$ , i.e. no binding is possible. The atomic density profile can now be explained by sampling the  $g_2(z)$  profile with well-defined binding distance over the ionic density distribution (see sketch in Fig. 3). While for (i) a spatially spread ion the molecular structure is hidden by the sampling, (ii) a localized ion reveals details of the binding by the two density peaks representing the strong bunching at distance  $d$ . In this way, we rediscover the onset of the central density hole predicted for a static ion [21, 22], however, here it is induced by the atom-ion interaction instead of originating from an external strong confinement. For  $N$  approaching  $N_c$ , one observes that the atom-ion correlation function broadens to larger relative distances which reduces the bunching at  $d$ . This corresponds to a spatial increase of the bound-state width. Beyond the dissociation point  $N_c$ , the strong suppression of larger atom-ion distances is lifted and the occurrence of the unbound fraction becomes prominent [see second maximum in Fig. 3 d)].

While the Gross ansatz is able to reproduce this behavior of  $g_2(z)$  qualitatively, it does not allow for population of an odd state due to the parity symmetry of the ground state. In Fig. 3, the population of the two bound states  $f_j = \langle \hat{a}_j^\dagger \hat{a}_j \rangle$  is shown with  $\hat{a}_j$  ( $\hat{a}_j^\dagger$ ) being their annihilation (creation) operators. We find a significant population of the second bound state in particular for even  $N$ . This excitation of atoms to the more weakly bound state allows to reduce the inter-atomic repulsive energy and hence stabilizes the many-body bound state. This explains the observed increase of  $N_c$  obtained from the correlated ML-MCTDHB results and can be viewed as the 1D analog of shell structure formation.

*Self-Localization.*— As previously seen, the increase of  $N$  localizes the ion. For a more quantitative analysis, we use the atomic ( $\sigma_A^2 = \langle \frac{1}{N} \sum_{i=1}^N z_i^2 \rangle$ ) and the ionic ( $\sigma_I^2 = \langle z_I^2 \rangle$ ) variance, shown in Fig. 4 in units of the non-interacting variance  $\sigma_0 = l/\sqrt{2}$ . Already for  $N < N_c$ , we observe that the ion as well as the atoms localize on a length scale smaller than the trap length. Since this is solely induced by the atom-ion interaction, we call it self-localization. For  $g = 0$ , both variances decrease monotonously with increasing  $N$ . Since in this case the state is an  $(N + 1)$ -body cluster, we can understand this self-localization solely by the increase of the total mass  $M = (N + 1)m$  localizing the center of mass wave func-

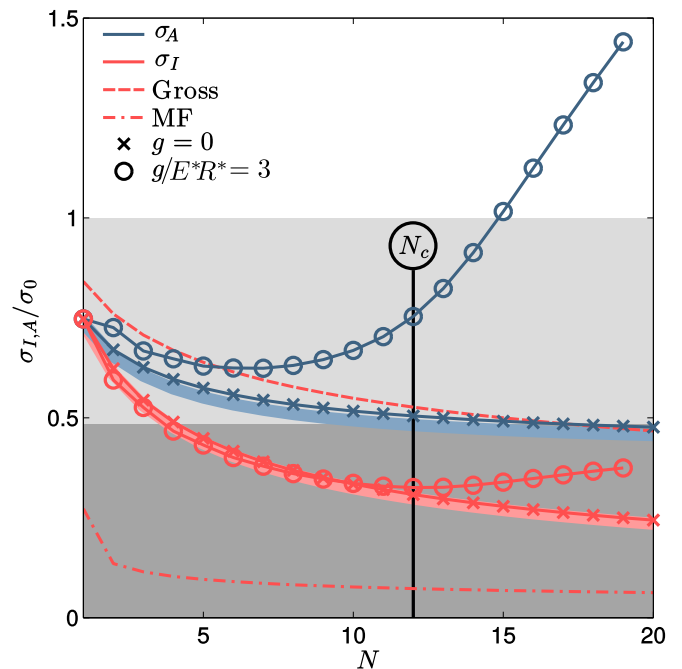


FIG. 4. (Color online) Self-localization. Variance of the atomic (blue) and the ionic (red) variance normalized by the non-interacting variance  $\sigma_0$ . Ionic variance from the Gross (dashed) and the mean-field (dashed dotted) ansatz for  $g = 0$  are shown, too. The light (light) thick lines represent  $\sigma_1$  ( $\sigma_A$ ) solely including the increase of  $M$  [26]. Dark (light) gray area represents the spatial extent of the bound states ( $\sigma_0$ ).

tion of the complete atom-ion system (thick lines; see Supplemental Material [26]). In this way, the atomic variance approaches the width of the bound state (dark gray area) because the static ion assumption becomes increasingly valid. Be aware that while the MF (dashed dotted line) strongly underestimates the ionic variance, the Gross ansatz strongly overestimates it (dashed line). For  $g > 0$ , the variance  $\sigma_A$  reveals a minimum and increases already for  $N < N_c$ . This goes hand in hand with the spatial widening of  $g_2$  [solid line in Fig. 3 d)] which we interpret as a broadening of the bound state. We emphasize that only when the effective bound state variance becomes comparable to the trap length the impact of the confinement on the molecular ion goes beyond the localization of the center of mass. In this case, one might think of a “molecule under pressure” [29, 30]. Beyond  $N_c$ , the ionic self-localization is reduced while the emergence of the shoulders in the atomic density gives rise to a rapid increase of  $\sigma_A$ . Here it becomes evident that the situation of equal trapping frequencies for atoms and ion represents no restriction to the generality of our results. Since the atoms and in particular the ion localize on distances smaller than their trapping length, the confining potentials only determine the center of mass variance. However, the atomic trap becomes indeed important for  $N > N_c$ , impacting the dissociation and defining the spatial extent of the unbound fraction. In contrast, the ion trap has actually vanishing impact such that it could in most cases even be switched off.

*Low energy excitations.*— In order to learn about the dynamical response of the strongly correlated ion within the bosonic ensemble to e.g. a quench of the ionic trap frequency, we introduce an effective single particle of mass  $m^*$  confined in a harmonic trap of frequency  $\omega^*$  [31]. Motivated by an ion density profile which is very well approximated by a Gaussian [26] and minor correlations between the ionic and the atomic IF coordinates, we use the particle associated to the ionic variable  $Z_I$  in the IF as effective particle. By construction, it has the equivalent density profile as the ion itself such that spatial measurements can be associated to both of them. From the Gross ansatz, one expects a free particle of mass  $m$  in a trap  $\omega\sqrt{1+N}$ . In order to obtain the effective frequency  $\omega^*$ , one could excite a breathing oscillation [32]. Here, however, we compute  $\omega^*$  from the spatial width  $l^* = \sqrt{\hbar/(m^*\omega^*)} (= \sqrt{2}\sigma_I)$  and the effective force exerted on the effective particle. Employing the knowledge of the full many-body wave function, the effective force  $F_I^*(Z_I)$  is given by the partial trace of the force operator  $F_I = -[\partial_{Z_I}, H]$  with  $H$  being the total system Hamiltonian in the IF [26].

The resulting  $m^*$  and  $\omega^*$  are shown in Fig. 5. In case all atoms are bound ( $N < N_c$ ), we observe that the effective ion accumulates a large mass, nearly the total mass  $M$ , increasing linear in  $N$ , while  $\omega^*$  is varying very little and is given approximatively by the trap frequency. Hence,

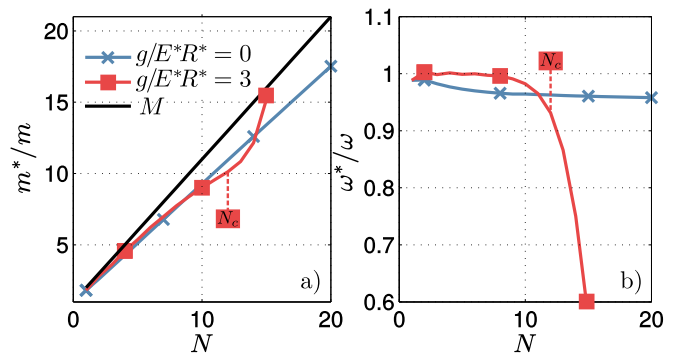


FIG. 5. (Color online) Effective ion behavior. a) Effective mass  $m^*/m$  and b) effective trapping frequency  $\omega^*/\omega$ . Note that the Gross ansatz gives  $\omega_G = \omega\sqrt{1+N}$  and  $m_G = m$ .

the localization can be understood by the generation of a huge effective mass. Approaching  $N_c$  for  $g/E^*R^* = 3$ ,  $m^*$  becomes sub-linear whereas for  $N > N_c$  it rapidly increases even to the total mass  $M$ . At the same time, the effective frequency strongly decreases revealing a slow response. Note that we do not give  $\omega^*$  and  $m^*$  for  $g = 3$  beyond  $N = 15$  because here the effective single particle picture breaks down [26]. We remark that small effective trapping frequencies and large effective masses are reminiscent of the behavior found for the ionic polaron in the strong coupling regime [12].

*Discussion and Experimental Realization.*— The attainment of the ultracold  $s$ -wave collision regime in atom-ion systems is under intense investigation [33–38]. The hybrid system can be created either by combination of atom and ion traps [34] or by fast ionization of a few atoms [33]. For instance, assuming a  $^{87}\text{Rb}^+$  ion in a  $^{87}\text{Rb}$  atomic cloud ( $R^* = 260\text{nm}$  and  $E^*/h = 1.6\text{kHz}$ ), our setup corresponds to a trap frequency of  $\omega \approx 2\pi \cdot 1.6\text{kHz}$ . With a transversal trapping frequency of  $\omega_\perp \approx 2\pi \cdot 50\text{kHz}$ , we obtain  $g \approx 1E^*R^*$  [39]. The formation of molecular ions, however, now relies on the occurrence of three-body collisions, the dominant reaction channel already at moderate densities [15], or can be induced by either photo-association [6] or a Raman-type scheme [13]. In this work, we have assumed that only the two most weakly bound states are of relevance for this reaction. This can be justified by the strong suppression of direct atom-capture into more deeply bound states [13]. Even though, these processes dictate the life-time of the molecular ion. Once the molecule is formed, it can be probed by measuring the atomic excess density near the ion [20, 21] or by wave-guide expansion [22]. Moreover, the binding can be identified via the effective ion mass by measuring the ionic variance [40] in the ground-state and during breathing dynamics.

*Conclusions.*— We have derived and characterized the many-body bound state of  $N$  atoms and a single ion both confined in a harmonic trap. The dissociation threshold



$N_c$  has been identified, for which a transition from an all-bound molecular ion to a molecule immersed into a background gas takes place. We have seen that even though the spatial extend of the particles is larger than the binding distance, one can identify the binding. The latter induces a substantial self-localization behavior for atoms and ion. Beyond that, we showed that the ion behaves like an effective particle of nearly the total mass in the bare ion trap. In addition, we were able to benchmark simplistic wave function classes via the ML-MCTDHB method, showing that correlations counteract the localization and stabilize the molecular cluster. Our results can be viewed as the basis for future intriguing studies concerning mesoscopic many-body bound states. A promising direction concerns the molecular formation process which can give a handle on formation time scales and stability. Directly related is the question regarding the energy and the structure of internal molecular excitations. Moreover, the insights gained into the structure of the many-body wave function can stimulate the design of a unifying, simple and predictive, theoretical model which captures the essential physics over the complete parameter regime even up to high atom numbers.

*Acknowledgements.*— The authors acknowledge inspiring conversations with Igor Lesanovsky and Zbigniew Idziaszek and helpful advice by Rene Gerritsma. Moreover, the authors thank Juliette Simonet for a detailed feedback on the manuscript. J.S. also thanks Sven Krönke and Valentin Bolsinger for many clarifying discussions and valuable suggestions. This work has been financially supported by the excellence cluster 'The Hamburg Centre for Ultrafast Imaging - Structure, Dynamics and Control of Matter at the Atomic Scale' of the Deutsche Forschungsgemeinschaft.

---

\* jschurer@physnet.uni-hamburg.de

† pschmelc@physnet.uni-hamburg.de

- [1] L. Meyer and F. Reif, *Phys. Rev.* **110**, 279 (1958).
- [2] K. R. Atkins, *Phys. Rev.* **116**, 1339 (1959).
- [3] E. Gross, *Ann. Phys. (N. Y.)* **19**, 234 (1962).
- [4] A. Härter and J. Hecker Denschlag, *Contemp. Phys.* **55**, 33 (2014).
- [5] L. Ratschbacher, C. Zipkes, C. Sias, and M. Köhl, *Nat. Phys.* **8**, 649 (2012).
- [6] A. Rakshit and B. Deb, *Phys. Rev. A* **83**, 022703 (2011).
- [7] A. Härter, A. Krüchow, A. Brunner, W. Schnitzler, S. Schmid, and J. H. Denschlag, *Phys. Rev. Lett.* **109**, 123201 (2012).
- [8] R. Côté, *Phys. Rev. Lett.* **85**, 5316 (2000).
- [9] L. Ratschbacher, C. Sias, L. Carcagni, J. M. Silver, C. Zipkes, and M. Köhl, *Phys. Rev. Lett.* **110**, 160402 (2013).
- [10] C. Zipkes, L. Ratschbacher, C. Sias, and M. Köhl, *New J. Phys.* **13**, 053020 (2011).
- [11] Z. Meir, T. Sikorsky, R. Ben-shlomi, N. Akerman, Y. Dalal, and R. Ozeri, *Phys. Rev. Lett.* **117**, 243401 (2016).
- [12] W. Casteels, J. Tempere, and J. T. Devreese, *J. Low Temp. Phys.* **162**, 266 (2010).
- [13] R. Côté, V. Kharchenko, and M. D. Lukin, *Phys. Rev. Lett.* **89**, 093001 (2002).
- [14] A. Krüchow, A. Mohammadi, A. Härter, J. H. Denschlag, J. Pérez-Ríos, and C. H. Greene, *Phys. Rev. Lett.* **116**, 193201 (2016).
- [15] A. Krüchow, A. Mohammadi, A. Härter, and J. Hecker Denschlag, *Phys. Rev. A* **94**, 030701 (2016).
- [16] R. V. Krems, W. C. Stwalley, and B. Friedrich, *Cold molecules : theory, experiment, applications* (CRC Press, 2009).
- [17] G. Quéméner and P. S. Julienne, *Chem. Rev.* **112**, 4949 (2012).
- [18] P. Stipanović, L. V. Markić, I. Bešlić, and J. Boronat, *Phys. Rev. Lett.* **113**, 253401 (2014).
- [19] B. Gao, *Phys. Rev. Lett.* **104**, 213201 (2010).
- [20] P. Massignan, C. J. Pethick, and H. Smith, *Phys. Rev. A* **71**, 023606 (2005).
- [21] J. Goold, H. Doerk, Z. Idziaszek, T. Calarco, and T. Busch, *Phys. Rev. A* **81**, 041601 (2010).
- [22] J. M. Schurer, P. Schmelcher, and A. Negretti, *Phys. Rev. A* **90**, 033601 (2014).
- [23] R. Gerritsma, A. Negretti, H. Doerk, Z. Idziaszek, T. Calarco, and F. Schmidt-Kaler, *Phys. Rev. Lett.* **109**, 080402 (2012).
- [24] J. M. Schurer, A. Negretti, and P. Schmelcher, *New J. Phys.* **17**, 083024 (2015).
- [25] J. M. Schurer, R. Gerritsma, P. Schmelcher, and A. Negretti, *Phys. Rev. A* **93**, 063602 (2016).
- [26] See Supplemental Material at [URL] for details on the atom-ion interaction, the frame transformations, the employed models, the effective force analysis, and for a discussion of convergence of our computational approach.
- [27] S. Krönke, L. Cao, O. Vendrell, and P. Schmelcher, *New J. Phys.* **15**, 063018 (2013).
- [28] L. Cao, S. Krönke, O. Vendrell, and P. Schmelcher, *J. Chem. Phys.* **139**, 134103 (2013).
- [29] D. Baye and K. D. Sen, *Phys. Rev. E* **78**, 026701 (2008).
- [30] C. Laughlin and S.-I. Chu, *J. Phys. A Math. Theor.* **42**, 265004 (2009).
- [31] As shown in Ref. [32] a trapped impurity may experience an effective potential.
- [32] J. Catani, G. Lamporesi, D. Naik, M. Gring, M. Inguscio, F. Minardi, A. Kantian, and T. Giamarchi, *Phys. Rev. A* **85**, 023623 (2012).
- [33] D. Ciampini, M. Anderlini, J. H. Müller, F. Fuso, O. Morsch, J. W. Thomsen, and E. Arimondo, *Phys. Rev. A* **66**, 043409 (2002).
- [34] A. T. Grier, M. Cetina, F. Oručević, and V. Vuletić, *Phys. Rev. Lett.* **102**, 223201 (2009).
- [35] S. Schmid, A. Härter, and J. H. Denschlag, *Phys. Rev. Lett.* **105**, 133202 (2010).
- [36] C. Zipkes, S. Palzer, C. Sias, and M. Köhl, *Nature* **464**, 388 (2010).
- [37] K. Ravi, S. Lee, A. Sharma, G. Werth, and S. A. Rangwala, *Appl. Phys. B* **107**, 971 (2012).
- [38] A. Lambrecht, J. Schmidt, P. Weckesser, M. Debatin, L. Karpa, and T. Schaetz, (2016), arXiv:1609.06429.
- [39] M. Olshani, *Phys. Rev. Lett.* **81**, 938 (1998).
- [40] R. Gerritsma, G. Kirchmair, F. Zähringer, E. Solano, R. Blatt, and C. F. Roos, *Nature* **463**, 68 (2010).